AGU100 ADVANCING EARTH AND SPACE SCIENCE

Geophysical Research Letters

RESEARCH LETTER
10.1029/2019GL085328

Transient Response of MJO Precipitation and Circulation to Greenhouse Gas Forcing

Hien X. Bui[1] and Eric D. Maloney[1]

[1]Department of Atmospheric Science, Colorado State University, Fort Collins, CO, USA

Key Points:
- Individual changes in MJO precipitation and circulation amplitude in RCP8.5 relative to the historical period only become detectable late in the 21st century
- Decreases in the ratio of MJO circulation to precipitation anomaly amplitude can be detected as early as 2021–2040
- Changes in the ratio of MJO circulation to precipitation anomaly amplitude are controlled by increased static stability that scales with global mean temperature changes

Supporting Information:
- Supporting Information S1

Correspondence to:
H. X. Bui,
hien.bui@colostate.edu

Citation:
Bui, H. X., & Maloney, E. D. (2019). Transient response of MJO precipitation and circulation to greenhouse gas forcing. *Geophysical Research Letters*, *46*, 13,546–13,555. https://doi.org/10.1029/2019GL085328

Received 9 SEP 2019
Accepted 9 NOV 2019
Accepted article online 22 NOV 2019
Published online 25 NOV 2019

Abstract Recent studies have shown that Madden-Julian oscillation (MJO) precipitation anomaly amplitude tends to increase while associated circulations weaken at the end of 21st century in Coupled Model Intercomparison Project phase 5 models under Representative Concentration Pathway 8.5. Transient changes of MJO characteristics earlier in the 21st century have received less attention. In this study, changes of MJO precipitation and circulation amplitude during these interim time periods under Representative Concentration Pathway 8.5 are examined in Coupled Model Intercomparison Project phase 5 models. Multimodel mean changes in MJO precipitation and circulation amplitude are not individually detectable in the early and middle 21st century relative to the historical period (1986–2005). However, robust multimodel mean decreases in the ratio of MJO wind to precipitation anomalies occur even early in the 21st century. This decreased ratio is explained by increasingly large tropical static stability as the climate warms, which under weak temperature gradient balance mandates that a diabatic heating anomaly is balanced by an increasingly weaker circulation anomaly. These results suggest the robustness of weak temperature gradient theory for explaining MJO dynamics, not only in an equilibrium climate but also in the transient response.

Plain Language Summary The strength of Madden-Julian oscillation (MJO) precipitation variations has previously been projected to increase while associated circulations weaken at the end of the 21st century under a pathway in which global radiative forcing reaches 8.5 W/m^2 by 2100. This paper examines projected changes in MJO characteristics during the early and middle of the 21st century in 11 coupled climate simulations. No detectable individual changes in the multimodel mean strength of MJO precipitation and associated circulations occur until the end of the 21st century. However, robust decreases in the relative strength of MJO wind to precipitation anomalies are detectable as early as 2021–2040. These decreases in the ratio of MJO wind to precipitation anomalies are successfully predicted under the assumption that horizontal temperature gradients in the tropical atmosphere are small, and using the fact that the tropical vertical dry static energy gradient increases with global mean temperature. Our results suggest the robustness of weak temperature gradient theory for explaining the dynamics of the MJO.

1. Introduction

The Madden-Julian oscillation (MJO; Madden & Julian, 1971, 1972) produces significant impacts on weather and climate phenomena over the tropics and extratropics, including a modulation of atmospheric rivers and hurricanes, among other impacts (Zhang, 2013, and references therein). Given these impacts of the MJO in current climate, an increasing interest exists in understanding how the MJO might change under global warming (Maloney et al., 2019). Global climate models (GCMs) generally find that MJO precipitation amplitude change ranges from −10% to +20% while MJO circulation strength increases at a slower rate or even weakens (by 1–10%) in the presence of substantial global mean temperature warming (Adames et al., 2017a, 2017b; Arnold et al., 2013, 2015; Bui & Maloney, 2018, 2019; Chang et al., 2015; Rushley et al., 2019; Takahashi et al., 2011). Bui and Maloney (2018) documented end of the 21st century (2081–2100) MJO precipitation and wind anomaly amplitude changes in several Coupled Model Intercomparison Project phase 5 (CMIP5) models forced with Representative Concentration Pathway 8.5 (RCP8.5) and explained the systematic weakening of MJO wind amplitude or lower rate of increase relative to precipitation amplitude through increases in tropical dry static stability using weak temperature gradient (WTG) theory (e.g., Sobel & Bretherton, 2000). In particular, WTG theory indicates weakening large-scale vertical motion per unit apparent heating given increases in tropical dry static stability in a warming climate (e.g., Wolding et al., 2016). A follow-up study suggested that changes in MJO precipitation amplitude at the end of the 21st century are regulated by competing effects from an increased lower tropospheric moisture

gradient and more top-heavy MJO diabatic heating profile with warming (Bui & Maloney, 2019). How the MJO changes in earlier decades of the 21st century (2021–2080) remains less thoroughly investigated, in particular how soon MJO changes in response to anthropogenic greenhouse gas (GHG) increases can be detected relative to the historical period given the nonlinear and chaotic nature of the climate system (e.g., Cassou et al., 2018; Kirtman, 2013).

Projecting future MJO changes is a challenging task owing to challenges GCMs have at simulating a realistic MJO in current climate (e.g., Ahn et al., 2017) and substantial internal variability in the climate system that may make conclusions drawn from single ensemble members misleading (e.g., Kirtman, 2013; Pohlmann et al., 2013; Shindell et al., 2012; Teng et al., 2011; Wigley et al., 2009). To address the first challenge, models can be prefiltered to select only those that produce a good MJO before doing projections. Hence, in the current study, we will analyze 11 CMIP5 simulations of the 21st century from models that have been assessed by Bui and Maloney (2018, 2019) and Rushley et al. (2019) to have a good MJO.

The second challenge arises from the fact that near-term climate projections are complicated by natural variability in the climate system that may cause uncertainty as to whether MJO precipitation and wind changes are produced by GHG forcing (e.g., Christensen, 2007; Hoerling et al., 2011; Kirtman, 2013; Meehl et al., 2013; Pohlmann et al., 2013). As discussed in the Intergovernmental Panel on Climate Change Fifth Assessment Report, the spread derived from CMIP5 models can be used as one tool to assess uncertainty in climate projections. In particular, a multimodel mean projected change can be assigned low confidence when it is smaller than internal variability estimated by the standard deviation of the change across all models (e.g., see Kirtman, 2013 Figures 11.10 and 11.12). Using this simple approach to assess uncertainty, we will explore whether a signal of MJO change can be detected against a background of natural internal variability in CMIP5 projections for the 21st century.

Aside from individual changes in MJO precipitation and wind amplitude, the change in the ratio of MJO wind to precipitation amplitude under global warming has also received much interest given that it helps us better understand the consequences of changes in MJO precipitation amplitude for teleconnections and wind-driven forcing of the ocean. Maloney and Xie (2013) showed that MJO wind variance changes can be predicted based on the precipitation variance changes if static stability increases are considered and a WTG assumption is used (see equation (1) below). Recent work with a broader set of models has supported this result. For example, changes in the ratio of MJO precipitation and wind variance at the end of 21st century in RCP8.5 are mediated by the increase in vertical dry static energy (DSE) gradient in the tropics, consistent with WTG theory (Bui & Maloney, 2018). However, it is unclear whether this relationship holds earlier in the 21st century.

In this paper, we build upon the results of Rushley et al. (2019), who assessed changes in the characteristics of MJO events in RCP8.5 over the 21st century, by including a broader suite of 11 CMIP5 simulations and through a compositing analysis. We also compare MJO changes to the historical period of 1986–2005 rather than a future 21st century base period as in Rushley et al. (2019) and place specific emphasis on changes in the relative strength of MJO circulation to precipitation anomalies.

2. Data and Methodology

2.1. Data

To provide confidence in future MJO projections, we use a subset of CMIP5 models that have been assessed to produce good MJO variability in current climate. Hence, we consider here the superset of CMIP5 models that were assessed in Bui and Maloney (2018, 2019) and Rushley et al. (2019) to produce good MJO variability in current climate. These include BCC-CSM1-1, CMCC-CMS, CMCC-CM, CNRM-CM5, GFDL-CM3, IPSL-CM5B-LR, MIROC5 (with three ensemble members), MRI-CGCM3, and NorESM1-M. Detailed model descriptions are given in Taylor et al. (2012). As documented in Henderson et al. (2017) and Rushley et al. (2019), these models produce relatively realistic eastward MJO propagation, a high ratio of eastward to westward spectral power, and realistically strong MJO amplitude. The number of models and ensemble members examined was limited by the availability of high-resolution temporal output.

To examine the transient response of the MJO, unless otherwise noted, we compare four 20-year periods in the 21st century (e.g., 2021–2040, 2041–2060, 2061–2080, and 2081–2100) in which the models are forced by

RCP8.5 to that of a historical period (1986–2005). In most of this paper, we focus on multimodel means and spread from the 11 simulations of 21st century warming listed above, with a specific focus on the boreal winter season (November–April) over the Indo-Pacific warm pool region (15°S–15°N, 60°E–180), although results from individual models are occasionally mentioned.

2.2. MJO Composites

To document MJO evolution in models, we generate composites based on the real-time multivariate MJO (RMM) indices, which are the principal components of the leading two combined empirical orthogonal functions (EOFs) of equatorial wind in the upper and lower troposphere and convection (Wheeler & Hendon, 2004). To do this, we project the models' band-pass filtered 30- to 90-day anomalies of outgoing longwave radiation and 250- and 850-hPa zonal winds averaged from 15°S to 15°N onto the observed multivariate EOFs (Wheeler & Hendon, 2004; can be downloaded at http://www.bom.gov.au/climate/mjo/). This technique allows direct comparison among all models and observations, and similar techniques have been used in multiple previous studies (e.g., Duffy et al., 2003; Henderson et al., 2017; Sperber, 2004; Sperber et al., 2005; Waliser, 2009). After obtaining the RMM indices, a composite evolution of the MJO is constructed for each 20-year period of interest in the RCP8.5 simulations over eight phases that represent the spatial location of the enhanced MJO convection as shown in Wheeler and Hendon (2004). The composite MJO anomaly fields for each phase are constructed from days when the RMM amplitude (i.e., $\sqrt{\mathrm{RMM1}^2 + \mathrm{RMM2}^2}$) is greater than 1. Note that we normalize the RMMs by a different standard deviation for each 20-year period of interest in the RCP8.5 and historical simulations for each model to reflect possible changes in MJO amplitude with climate changes. However, results are similar when using a common standard deviation calculated across all times.

In addition to conducting RMM analysis by projection onto the observed multivariate EOFs, we also repeated the analysis by computing multivariate EOFs separately for each model and time period. This alternate method helps mitigate concerns about spatial shifts in MJO variance that might occur due to changes in the pattern of sea surface temperature (SST) and other thermodynamic factors with warming (e.g., Bui & Maloney, 2018; Xie et al., 2010). The results of this alternative method of deriving RMM indices are consistent with those derived from projection onto the observed EOFs, and so we only show the latter results here.

3. Results

The amplitude of composite MJO fields is initially assessed for each 20-year period by computing the root-mean-square of composite fields at each location for each model over all eight MJO phases. Figure 1 shows the multimodel mean spatial pattern of MJO precipitation (left column) and 500-hPa omega (right column) amplitude for the historical simulation (1986–2005) and the difference of four 20-year periods of the 21st century RCP8.5 simulation (2021–2040, 2041–2060, 2061–2080, and 2081–2100) and the historical simulation. The strongest MJO precipitation and 500-hPa omega anomalies in the historical simulation are found in the western Pacific and Indian Oceans, consistent with previous studies and observations (Figures 1a and 1f; Bui & Maloney, 2018, and reference therein). Multimodel mean projected MJO precipitation changes show a modest decrease in the early 21st century, and increases in the later decades of century, especially near the Maritime Continent. Tropical eastern Pacific increases in MJO precipitation amplitude are also noted at the end of the 21st century. However, these multimodel mean regional changes, especially earlier in the 21st century, are not significant given the large multimodel variability (see Figures S1, S2, and S3 in the supporting information). For composite 500-hPa omega amplitude, a modest weakening is apparent in the early decades of the century in approximately the same location as that of the precipitation amplitude changes. The similar-signed changes between precipitation and wind early in the century are consistent with modest early century static stability changes, a point discussed in more detail in the context of Figures 2–4 below. MJO omega amplitude weakens even further toward the end of the century. We note that the end of 21st century results showing an increase in MJO precipitation amplitude and decreases in MJO circulation amplitude are consistent with our previous studies (e.g., Bui & Maloney, 2018, 2019) and discussed in more detail below, although here we analyze about twice as many simulations. The pattern of omega amplitude change at the end of the 21st century is generally consistent with the precipitation amplitude change acting in concert with increases in tropospheric static stability. This was tested by predicting the distribution of omega amplitude change given the static stability and precipitation amplitude changes (not shown here).

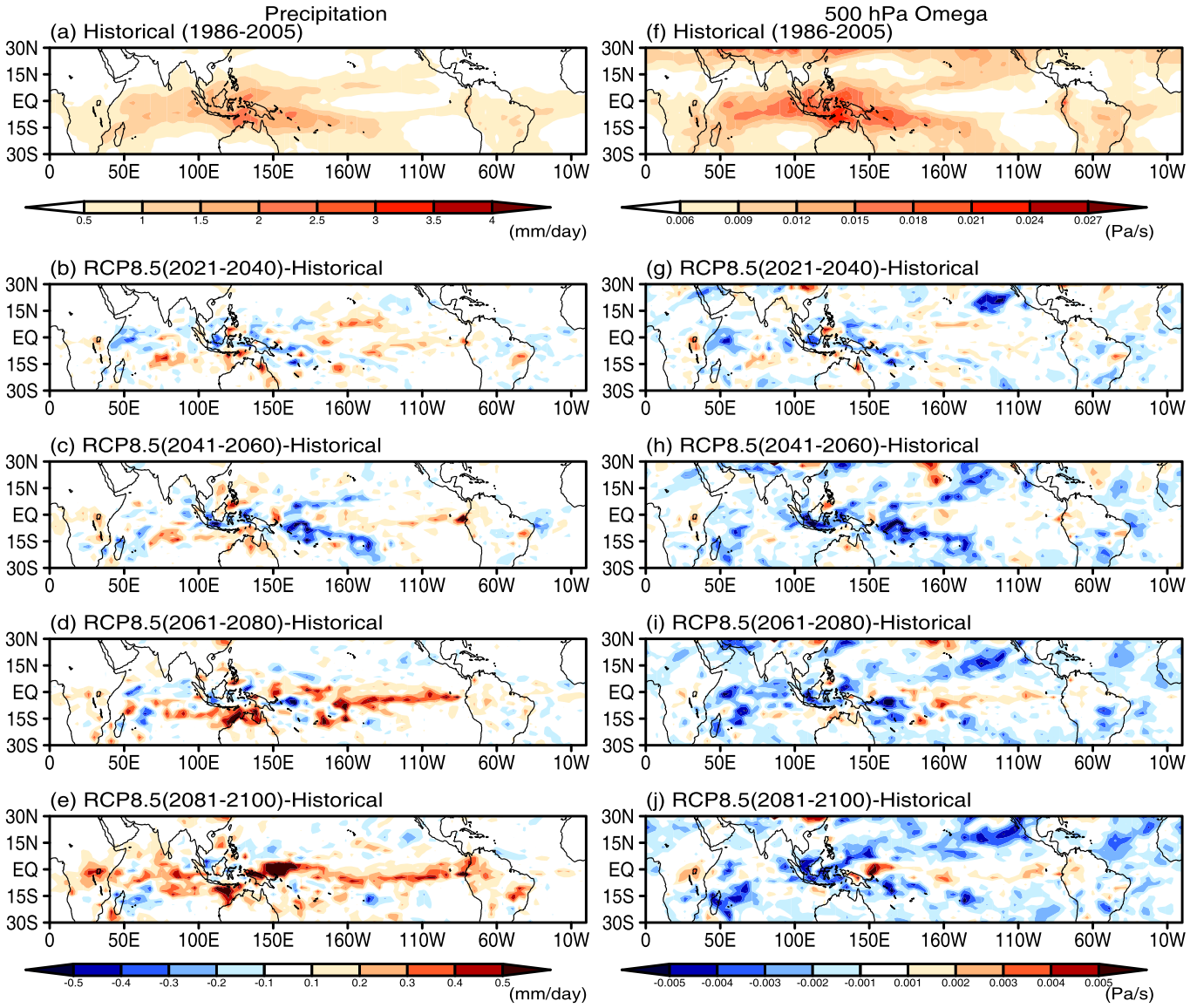

Figure 1. The top row shows multimodel mean amplitude of MJO precipitation (left panels, units are mm/day) and 500 hPa omega (right panels, Pa/s) for the historical period. The bottom four rows represent the difference relative to the historical period for different decades of the 21st century (e.g., 2021–2040, 2041–2060, 2061–2080, and 2081–2100).

To better quantify MJO changes over the warm pool region of the Indo-Pacific Ocean, Figures 2a and 2b display the multimodel mean MJO amplitude change shown in Figure 1 averaged over 15°S-15°N, 60°E–180°E, where MJO precipitation and wind variability in the present climate is concentrated. We note that results are not sensitive to the exact averaging bounds used. The thick bars in Figure 2 show the fractional change relative to the average of the historical period plus the period of interest (e.g., fractional change of precipitation [P] at the early of 21st century [2021–2040] relative to historical [1986–2005] simulation is calculated as $[P_{2021–2040} - P_{1986–2005}]/[[P_{2021–2040} + P_{1986–2005}]/2]$). The standard deviation across models is represented by lines. Inspired by the method used in Chapter 11 of the Intergovernmental Panel on Climate Change Fifth Assessment Report (Kirtman, 2013), we consider a change in MJO amplitude to be detectable relative to the historical period if the multimodel mean change is greater than the standard deviation of the change across models, assuming the latter has a substantial component associated with decadal variability in the climate system. Until 2080, both MJO precipitation and 500-hPa omega amplitude show small fractional

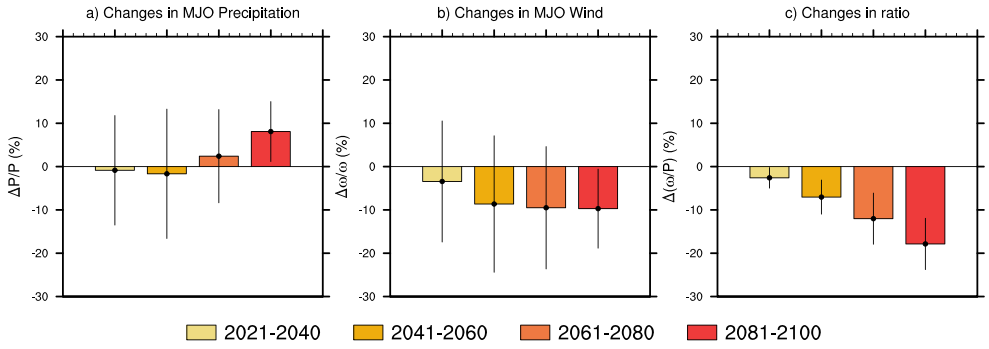

Figure 2. Multimodel mean fractional changes in (a) MJO precipitation and (b) 500-hPa omega amplitude, and (c) changes in the ratio between the two in different decades of the 21st century relative to the historical simulation averaged over the warm pool region (15°S–15°N, 60°E–180). The bars represent the standard deviation across models. Units are in percent.

changes and fall within the one standard deviation bounds, suggesting no detectable change in MJO precipitation and circulation amplitude when considered separately. At the end of the 21st century, however, both MJO precipitation and wind amplitude changes indicate a multimodel mean change that is

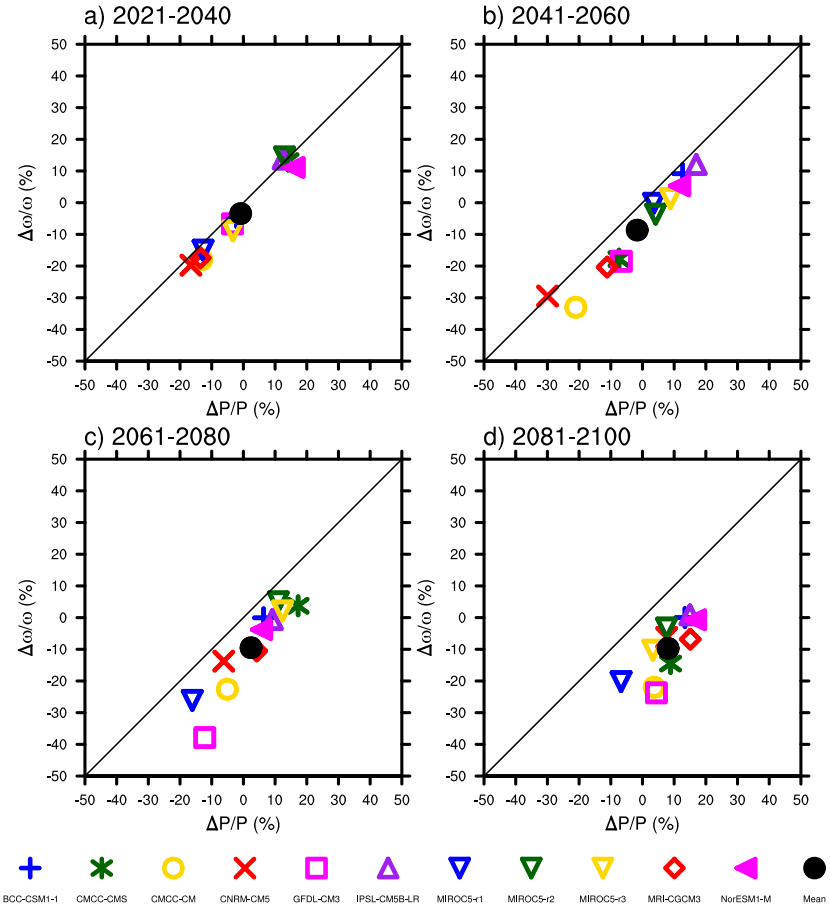

Figure 3. Scatterplots of 500-hPa omega amplitude change (*y* axis) and MJO precipitation amplitude change (*x* axis) for individual CMIP5 models for different decades of the 21st century relative to the historical simulation. Units are in percent.

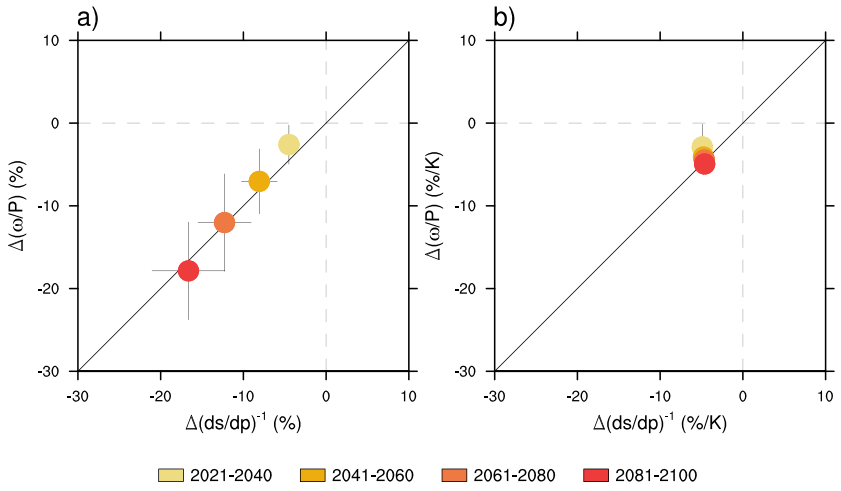

Figure 4. Multimodel mean changes in the ratio between MJO 500-hPa omega and precipitation amplitude (*y* axis) versus the inverse vertical dry static energy (DSE) gradient averaged from 850 to 200 hPa (*x* axis) from different decades of the 21st century relative to the historical. The bars represent the standard deviation calculated across all models. Units are shown in percent and % K^{-1} in Figures 4a and 4b, respectively.

larger than the model spread, suggesting the emergence of a signal of increased MJO precipitation variability and reduced wind variability. This end of the 21st century result is consistent with Bui and Maloney (2018, 2019). The spatial distribution of these changes indicates noisier patterns (Figure S1) but is consistent with the domain average.

The results of Figures 2a and 2b suggesting the importance of internal variability in regulating near-term MJO changes relative to anthropogenic forcing, and that the impact of MJO on many weather and climate phenomena in a future climate may weaken per unit precipitation anomaly due to relatively weaker large-scale circulations (Bui & Maloney, 2018). This contention is supported by an analysis of the 500-hPa omega and precipitation amplitude changes from the individual simulations (Figure 3), which highlight the lack of consistency in sign and amplitude of MJO wind and precipitation changes early in the 21st century. Individual models can exhibit a different sign of amplitude changes from one decade to the next, especially before 2080. The three ensemble members from MIROC5 do not even agree on the sign of 500 hPa and precipitation amplitude changes for three of the four 20-year periods (e.g., 2061–2080). However, the models start to converge toward increases in MJO precipitation amplitude and decreases in MJO wind amplitude in the last decades of 21st century. In the early part of the 21st century, MJO wind and precipitation anomaly changes in models approximately scale with each other (i.e., fall along a one-to-one line), while later in the century changes in the strength of MJO circulation anomalies do not keep up with precipitation amplitude increases. Signals in the relative strength of MJO circulation and precipitation anomalies will be examined next.

Interestingly, even though changes in MJO wind and precipitation amplitude are not detectable until 2081–2100, changes in ratio of these two quantities are detectable early in the 21st century (Figure 2c), with MJO circulation amplitude per unit precipitation being reduced. The ratio between the root-mean-square of composite 500-hPa omega and precipitation anomalies is calculated for each model before computing a difference relative to the historical period and before calculating the multimodel mean. Changes in the ratio of MJO wind to precipitation amplitude decrease approximately linearly, from about −2% in the early century to approximately −17% in the late century. This reduction implies consequences for MJO teleconnections to the remote tropics and extratropics, since wind anomalies would be reduced relative to current climate for the same strength precipitation anomaly. If MJO activity is diagnosed using a simple standard deviation of 30–90 day and eastward wave numbers 1–5 filtered data (Figures S2 and S3 in the supporting information), changes in the ratio of MJO wind to precipitation amplitude are similarly robust, although precisely when precipitation and wind amplitude changes become individually detectable does depend on the analysis technique.

To help explain why the ratio of MJO circulation to precipitation anomalies changes in a warmer climate, we invoke static stability changes. According to WTG theory, diabatic heating and wind can be related as (e.g., Sobel & Bretherton, 2000)

$$Q \approx \omega \frac{\partial s}{\partial p} \tag{1}$$

where Q is apparent heat source that is approximately proportional to precipitation anomalies in MJO convective regions, ω is pressure velocity, and $\frac{\partial s}{\partial p}$ is the vertical DSE gradient ($s = C_p T + gz$ where T is temperature, g is gravity, z is height, and C_p is the specific heat of dry air at constant pressure). Wolding et al. (2016) showed that to good approximation, the DSE gradient can be represented by the climatological mean while the other two variables in 1 represent the MJO timescale. To understand Figure 2c, 1 can be reorganized such that the ratio of MJO vertical velocity and diabatic heating anomalies is proportional to the inverse of the vertical DSE gradient (Bui & Maloney, 2018; Maloney & Xie, 2013). The vertical DSE gradient scales with increases in surface temperature and boundary layer humidity given greater warming aloft, assuming that the vertical temperature profile in the tropics is a moist adiabat (Bui & Maloney, 2019; Held & Soden, 2006; Knutson & Manabe, 1995). In the early 21st century, changes in SST, tropospheric temperature, and static stability are small but detectable (e.g., Kirtman, 2013; Meehl et al., 2010), so changes in the ratio of MJO wind to precipitation anomalies are initially detectable but modest (Figure 2c). In the later decades, when the SST and static stability changes become large (e.g., Collins, 2013), the change in the ratio of circulation and precipitation anomalies reaches about −17% in 2081–2100.

To reinforce whether the WTG assumption can be used to explain the relative changes of MJO precipitation and circulation over the 21st century, Figure 4 shows scatterplots of changes in the ratio between MJO 500-hPa omega and precipitation amplitude versus changes in the inverse of the vertical DSE gradient. Changes in tropospheric static stability gradient are calculated using climatological mean fields over the respective 20-year time periods, averaged from 850 to 200 hPa. Inverse DSE gradient changes range from −4% to −17% over the century, with a change in static stability detectable as early as 2021–2040 relative to the historical period when the multimodel mean change is greater than the standard deviation of the changes across models. The change in ratio of MJO omega to precipitation amplitude is detectable by 2021–2040 and is well predicted by the inverse static stability change. This result implies the robustness of WTG theory for explaining the relationship between MJO wind and precipitation anomalies in the transient response to climate change (Figure 4a).

Figure 4b shows an analogous scatterplot to Figure 4a, except with normalization by the global mean surface temperature change. The changes for all decades collapse to around $-4\%\ K^{-1}$ for both the inverse DSE gradient change and change in ratio between omega and precipitation. Examination of individual models (Figures S4 and S5 in the supporting information) also shows that changes in the ratio between precipitation and wind versus inverse DSE gradient changes cluster near a line of slope one.

In addition to the analysis of MJO precipitation and 500-hPa omega anomalies above, we also assessed changes in MJO 850-hPa zonal wind. They are generally consistent with those from omega, although noisier (not shown). We also examined the changes in MJO precipitation and wind amplitude from one model (BCC-CSM1-1) that has an RCP8.5 simulation to year 2300 with available high temporal resolution output. The change in the ratio between MJO 500-hPa omega and precipitation amplitude versus change in the inverse of DSE gradient shows a remarkable linear relationship to the end of the 23rd century (Figure S6 in the supporting information), with decreases in the ratio of about 30% by 2281–2300.

4. Conclusions

We have analyzed the historical and the 21st century RCP8.5 simulations from 11 CMIP5 simulations with high MJO simulation skill in order to understand the transient climate response of MJO precipitation and circulation to GHG forcing. We examined the changes of MJO precipitation and 500-hPa omega in four 20-year periods (e.g., 2021–2040, 2041–2060, 2061–2080, and 2081–2100) relative to a historical period (1986–2005) and also used the climatological mean DSE gradient change to predict the change in the ratio of MJO omega and precipitation. Our primary conclusions are as follows.

1. Changes to the amplitude of MJO precipitation and circulation anomalies are not individually detectable until the end of the 21st century as the multimodel mean is smaller than the standard deviation across models, suggesting the importance of internal variability for regulating near-term MJO changes (see Figures 2a, 2b, and 3).
2. Changes in the ratio of MJO 500-hPa omega to precipitation anomaly amplitude are detectable as early as 2021–2040 (see Figure 2c).
3. Changes in the ratio of MJO circulation to precipitation anomaly amplitude are consistent with changes in the inverse vertical DSE gradient, suggesting the importance of WTG theory for understanding the transient climate response to anthropogenic forcing (see Figures 4 and S6 in the supporting information).

Our results suggest that even though changes in MJO wind and precipitation anomalies may not be individually detectable until the end of the 21st century if the climate warms following a path like RCP8.5, changes in the relative amplitudes of MJO wind and precipitation anomalies may be detectable much sooner. It is possible that such changes are already be detectable in the satellite precipitation and reanalysis and sounding wind record since 1979, given that the global mean surface temperature has warmed by about 0.8 °C since then. We plan to examine this in future work.

The current study is only a first step in assessing the transient climate response of the MJO as CMIP5 RCP8.5 simulations combine both the direct effects from GHG forcing and those from the thermal response of the climate system to this forcing. In future modeling work, we will try to separate the MJO climate change response associated with these two different factors. When a carbon dioxide (CO_2) increase is made in the atmosphere, its radiative forcing leads to a rapid tropospheric temperature adjustment before the surface has had time to substantially warm. These adjustments can increase atmospheric stability, reduce convection, and lead to a reduction in precipitation (e.g., Gregory & Webb, 2008; Kamae & Watanabe, 2013; Merlis, 2015; Yang et al., 2003). The reduction of climatological mean precipitation in direct response to GHG forcing has been considered in the CMIP5 multimodel mean (Bony et al., 2013) and in the model sensitivity experiments that separately examine fast (surface temperature-independent) and slow (surface temperature-dependent) responses to forcing (e.g., Andrews et al., 2012; Andrews & Forster, 2010; Bala et al., 2010; Chadwick et al., 2014). The conflicting effects from GHG versus aerosols in modulating the climate response of the MJO should also be considered, as has been assessed for other tropical phenomena (e.g., Sobel et al., 2019).

Acknowledgments
We acknowledge support from the Climate and Large-Scale Dynamics program of the National Science Foundation under grant AGS-1841754, and from NOAA MAPP, CVP, and OWAQ grants NA18OAR4310268, NA18OAR4310299, and NA19OAR4590151, respectively. We thank the World Climate Research Programmes (WCRP) Working Group for providing the CMIP5 data, which can be downloaded at https://esgf-node.llnl.gov/projects/cmip5/.

References

Adames, Á. F., Kim, D., Sobel, A. H., Del Genio, A., & Wu, J. (2017a). Changes in the structure and propagation of the MJO with increasing CO_2. *Journal of Advances in Modeling Earth Systems*, *9*, 1251–1268. https://doi.org/10.1002/2017MS000913

Adames, Á. F., Kim, D., Sobel, A. H., Del Genio, A., & Wu, J. (2017b). Characterization of moist processes associated with changes in the propagation of the MJO with increasing CO_2. *Journal of Advances in Modeling Earth Systems*, *9*, 2946–2967. https://doi.org/10.1002/2017MS001040

Ahn, M.-S., Kim, D., Sperber, K., Maloney, E., Waliser, D., & Hendon, H. (2017). MJO simulation in CMIP5 climate models: MJO skill metrics and process-oriented diagnosis. *Climate Dynamic*, *49*, 4023. https://doi.org/10.1007/s00382-017-3558-4

Andrews, T., & Forster, P. M. (2010). The transient response of global-mean precipitation to increasing carbon dioxide levels. *Environmental Research Letters*, *5*(2).

Andrews, T., Gregory, J. M., Webb, M. J., & Taylor, K. E. (2012). Forcing, feedbacks and climate sensitivity in CMIP5 coupled atmosphere-ocean climate models. *Geophysical Research Letter*, *39*, L09712. https://doi.org/10.1029/2012GL051607

Arnold, N. P., Branson, M., Kuang, Z., Randall, D. A., & Tziperman, E. (2015). MJO intensification with warming in the superparameterized CESM. *Journal of Climate*, *28*(7), 2706–2724. https://doi.org/10.1175/JCLI-D-14-00494.1

Arnold, N. P., Kuang, Z., & Tziperman, E. (2013). Enhanced MJO-like variability at high SST. *Journal of Climate*, *26*(3), 988–1001. https://doi.org/10.1175/JCLI-D-12-00272.1

Bala, G., Caldeira, K., & Nemani, R. (2010). Fast versus slow response in climate change: Implications for the global hydrological cycle. *Climate Dynamics*, *35*(2-3), 423–434. https://doi.org/10.1007/s00382-009-0583-y

Bony, S., Bellon, G., Klocke, D., Sherwood, S., Fermepin, S., & Denvil, S. (2013). Robust direct effect of carbon dioxide on tropical circulation and regional precipitation. *Nature Geoscience*, *6*, 447. https://doi.org/10.1038/ngeo1799

Bui, H. X., & Maloney, E. D. (2018). Changes in Madden-Julian oscillation precipitation and wind variance under global warming. *Geophysical Research Letters*, *45*, 7148–7155. https://doi.org/10.1029/2018GL078504

Bui, H. X., & Maloney, E. D. (2019). Mechanisms for global warming impacts on Madden-Julian oscillation precipitation amplitude. *Journal of Climate*, *32*, 6961–6975. https://doi.org/10.1175/JCLI-D-19-0051.1

Cassou, C., Kushnir, Y., Hawkins, E., Pirani, A., Kucharski, F., Kang, I., & Caltabiano, N. (2018). Decadal climate variability and predictability: Challenges and opportunities. *Bulletin of the American Meteorological Society*, *99*, 479–490. https://doi.org/10.1175/BAMS-D-16-0286.1

Chadwick, R., Good, P., Andrews, T., & Martin, G. (2014). Surface warming patterns drive tropical rainfall pattern responses to CO_2 forcing on all timescales. *Geophysical Research Letter*, *41*, 610–615. https://doi.org/10.1002/2013GL058504

Chang, C.-W. J., Tseng, W.-L., Hsu, H.-H., Keenlyside, N., & Tsuang, B.-J. (2015). The Madden-Julian oscillation in a warmer world. *Geophysical Research Letters*, *42*, 6034–6042. https://doi.org/10.1002/2015GL065095

Christensen, J. H. (2007). Regional climate projection. In S. Solomon et al. (Eds.), *Climate change 2007: The physical science basis. Contribution of Working Group I to the Fourth Assessment Report of the Intergovernmental Panel on Climate Change* (pp. 847–940). Cambridge, United Kingdom and New York, NY, USA: Cambridge University Press.

Collins, M. R. (2013). Long-term climate change: Projections, commitments and irreversibility. In T. F. Stocker et al. (Eds.), *Climate change 2013: The physical science basis. Contribution of Working Group I to the Fifth Assessment Report of the Intergovernmental Panel on Climate Change* (pp. 1029–1136). Cambridge, United Kingdom and New York, NY, USA: Cambridge University Press.

Duffy, P. B., Govindasamy, B., Iorio, J. P., Milovich, J., Sperber, K. R., Taylor, K. E., et al. (2003). High-resolution simulations of global climate, part 1: Present climate. *Climate Dynamics*, *21*(5), 371–390. https://doi.org/10.1007/s00382-003-0339-z

Gregory, J., & Webb, M. (2008). Tropospheric adjustment induces a cloud component in CO_2 forcing. *Journal of Climate*, *21*(1), 58–71. https://doi.org/10.1175/2007JCLI1834.1

Held, I. M., & Soden, B. J. (2006). Robust responses of the hydrological cycle to global warming. *Journal of Climate*, *19*(21), 5686–5699. https://doi.org/10.1175/JCLI3990.1

Henderson, S. A., Maloney, E. D., & Son, S.-W. (2017). Madden-Julian oscillation Pacific teleconnections: The impact of the basic state and MJO representation in general circulation models. *Journal of Climate*, *30*(12), 4567–4587. https://doi.org/10.1175/JCLI-D-16-0789.1

Hoerling, M., Hurrell, J., Kumar, A., Terray, L., Eischeid, J., Pegion, P., et al. (2011). On North American decadal climate for 2011–20. *Journal of Climate*, *24*(16), 4519–4528. https://doi.org/10.1175/2011JCLI4137.1

Kamae, Y., & Watanabe, M. (2013). Tropospheric adjustment to increasing CO_2: Its timescale and the role of land–sea contrast. *Climate dynamics*, *41*(11-12), 3007–3024. https://doi.org/10.1007/s00382-012-1555-1

Kirtman, B. (2013). Near-term climate change: Projections and predictability. In T. F. Stocker et al. (Eds.), *Climate change 2013: The physical science basis. Contribution of Working Group I to the Fifth Assessment Report of the Intergovernmental Panel on Climate Change* (pp. 953–1028). Cambridge, United Kingdom and New York, NY, USA: Cambridge University Press.

Knutson, T. R., & Manabe, S. (1995). Time-mean response over the tropical Pacific to increased CO2 in a coupled ocean–atmosphere model. *Journal of Climate*, *8*(9), 2181–2199. https://doi.org/10.1175/1520-0442(1995)008<2181:TMROTT>2.0.CO;2

Madden, R. A., & Julian, P. R. (1971). Detection of a 40–50 day oscillation in the zonal wind in the tropical Pacific. *Journal of the Atmospheric Sciences*, *28*(5), 702–708. https://doi.org/10.1175/1520-0469(1971)028<0702:DOADOI>2.0.CO;2

Madden, R. A., & Julian, P. R. (1972). Description of global-scale circulation cells in the tropics with a 40–50 day period. *Journal of the Atmospheric Sciences*, *29*(6), 1109–1123. https://doi.org/10.1175/1520-0469(1972)029<1109:DOGSCC>2.0.CO;2

Maloney, E. D., Adames, Á. F., & Bui, H. X. (2019). Madden-Julian oscillation changes under anthropogenic warming. *Nature Climate Change*, *9*(1), 26–33. https://doi.org/10.1038/s41558-018-0331-6

Maloney, E. D., & Xie, S.-P. (2013). Sensitivity of tropical intraseasonal variability to the pattern of climate warming. *Journal of Advances in Modeling Earth Systems*, *5*, 32–47. https://doi.org/10.1029/2012MS000171

Meehl, G. A., Goddard, L., Boer, G., Burgman, R., Branstator, G., Cassou, C., et al. (2013). Decadal climate prediction: An update from the trenches. *Bulletin of the American Meteorological Society*, *95*(2), 243–267. https://doi.org/10.1175/BAMS-D-12-00241.1

Meehl, G. A., Hu, A., & Tebaldi, C. (2010). Decadal prediction in the Pacific region. *Journal of Climate*, *23*, 2959–2973. https://doi.org/10.1175/2010JCLI3296.1

Merlis, T. M. (2015). Direct weakening of tropical circulations from masked CO_2 radiative forcing. *Proceedings of the National Academy of Sciences*, *112*(43), 13,167–13,171. https://doi.org/10.1073/pnas.1508268112

Pohlmann, H., Smith, D. M., Balmaseda, M. A., Keenlyside, N. S., Masina, S., Matei, D., et al. (2013). Predictability of the mid-latitude Atlantic meridional overturning circulation in a multi-model system. *Climate Dynamic*, *41*(3-4), 775–785. https://doi.org/10.1007/s00382-013-1663-6

Rushley, S. S., Kim, D., & Adames, Á. F. (2019). Changes in the MJO under greenhouse gas-induced warming in CMIP5 models. *Journal of Climate*, *32*(3), 803–821. https://doi.org/10.1175/JCLI-D-18-0437.1

Shindell, D., Kuylenstierna, J. C. I., Vignati, E., van Dingenen, R., Amann, M., Klimont, Z., et al. (2012). Simultaneously mitigating near-term climate change and improving human health and food security. *Science*, *335*(6065), 183–189. https://doi.org/10.1126/science.1210026

Sobel, A. H., & Bretherton, C. S. (2000). Modeling tropical precipitation in a single column. *Journal of Climate*, *13*(24), 4378–4392. https://doi.org/10.1175/1520-0442(2000)013<4378:MTPIAS>2.0.CO;2

Sobel, A. H., Camargo, S. J., & Previdi, M. (2019). Aerosol vs. greenhouse gas effects on tropical cyclone potential intensity and the hydrologic cycle. *Journal of Climate*, *32*(17), 5511–5527. https://doi.org/10.1175/JCLI-D-18-0357.1

Sperber, K. R. (2004). Madden-Julian variability in NCAR CAM2.0 and CCSM2.0. *Climate Dynamics*, *23*(3), 259–278. https://doi.org/10.1007/s00382-004-0447-4

Sperber, K. R., Gualdi, S., Legutke, S., & Gayler, V. (2005). The Madden–Julian oscillation in ECHAM4 coupled and uncoupled general circulation models. *Climate Dynamics*, *25*(2), 117–140. https://doi.org/10.1007/s00382-005-0026-3

Takahashi, C., Sato, N., Seiki, A., Yoneyama, K., & Shirooka, R. (2011). Projected future change of MJO and its extratropical teleconnection in East Asia during the northern winter simulated in IPCC AR4 models. *Science Online Letters on the Atmosphere*, *7*, 201–204. https://doi.org/10.2151/sola.2011-051

Taylor, K. E., Stouffer, R. J., & Meehl, G. A. (2012). An overview of CMIP5 and the experiment design. *Bulletin of the American Meteorological Society*, *93*(4), 485–498. https://doi.org/10.1175/BAMS-D-11-00094.1

Teng, H. Y., Branstator, G., & Meehl, G. A. (2011). Predictability of the Atlantic overturning circulation and associated surface patterns in two CCSM3 climate change ensemble experiments. *Journal of Climate*, *24*, 6054–6076. https://doi.org/10.1175/2011JCLI4207.1

Waliser, D. (2009). MJO simulation diagnostics. *Journal of Climate*, *22*(11), 3006–3030. https://doi.org/10.1175/2008JCLI2731.1

Wheeler, M. C., & Hendon, H. H. (2004). An all-season real-time multivariate MJO index: Development of an index for monitoring and prediction. *Monthly Weather Review*, *132*(8), 1917–1932. https://doi.org/10.1175/1520-0493(2004)132<1917:AARMMI>2.0.CO;2

Wigley, T. M. L., Clarke, L. E., Edmonds, J. A., Jacoby, H. D., Paltsev, S., Pitcher, H., et al. (2009). Uncertainties in climate stabilization. *Climatic Change*, *97*(1-2), 85–121. https://doi.org/10.1007/s10584-009-9585-3

Wolding, B. O., Maloney, E. D., & Mark, B. (2016). Vertically resolved weak temperature gradient analysis of the Madden-Julian oscillation in SP-CESM. *Journal of Advances in Modeling Earth Systems*, *8*, 1586–1619. https://doi.org/10.1002/2016MS000724

Xie, S.-P., Deser, C., Vecchi, G. A., Ma, J., Teng, H., & Wittenberg, A. T. (2010). Global warming pattern formation: Sea surface temperature and rainfall. *Journal of Climate*, *23*(4), 966–986. https://doi.org/10.1175/2009JCLI3329.1

Yang, F., Kumar, A., Schlesinger, M. E., & Wang, W. (2003). Intensity of hydrological cycles in warmer climates. *Journal of Climate*, *16*(14), 2419–2423. https://doi.org/10.1175/2779.1

Zhang, C. (2013). Madden–Julian oscillation: Bridging weather and climate. *Bulletin of the American Meteorological Society*, *94*(12), 1849–1870. https://doi.org/10.1175/BAMS-D-12-00026.1